

# Enhanced Extractor-Selector Framework and Symmetrization Weighted Binary Cross-Entropy for Edge Detections

Hao Shu

## Abstract

Recent advancements have demonstrated the effectiveness of the extractor-selector (E-S) framework in edge detection (ED) tasks, which achieves state-of-the-art (SOTA) performance in both quantitative metrics and perceptual quality. However, this method still falls short of fully exploiting the potential of feature extractors, as selectors only operate on highly compressed feature maps that lack diversity and suffer from substantial information loss. Additionally, while union training can improve perceptual quality, the highest evaluation scores are typically obtained without it, creating a trade-off between quantitative accuracy and perceptual fidelity. To address these limitations, we propose an enhanced E-S architecture, which utilizes richer, less-loss feature representations and incorporates auxiliary features during the selection process, thereby improving the effectiveness of the feature selection mechanism. Additionally, we introduce a novel loss function, the Symmetrization Weight Binary Cross-Entropy (SWBCE), which simultaneously emphasizes both the recall of edge pixels and the suppression of erroneous edge predictions, thereby enhancing the predictions both in the perceptual quality and the prediction accuracy. The effectiveness and superiority of our approaches over baseline models, the standard E-S framework, and the standard Weight Binary Cross-Entropy (WBCE) loss function are demonstrated by extensive experiments. For example, our enhanced E-S architecture trained with SWBCE loss function achieves average improvements of 8.25%, 8.01%, and 33.25% in ODS, OIS, and AP, measured on BIPED2 compared with the baseline models, significantly outperforming the standard E-S method. The results set new benchmarks for ED tasks, and highlight the potential of the methods in beyond.

## 1 Introduction

Edge detection (ED) is a foundational problem in computer vision, with widespread applications in higher-level tasks

such as image inpainting [Nazeri *et al.*, 2019], object detection [Zhan *et al.*, 2007], and image segmentation [Muthukrishnan and Radha, 2011]. Over the past decade, deep learning methods such as convolutional neural networks (CNNs) have substantially advanced ED by enabling the extraction of hierarchical, discriminative features directly from data. These data-driven techniques have significantly improved performance on benchmark datasets. Notable works such as Holistically-Nested Edge Detection (HED) [Xie and Tu, 2015], Bi-Directional Cascade Network (BDCN) [He *et al.*, 2022], and Dense Extreme Inception Network (Dexi) [Soria *et al.*, 2023b] have set new performance standards by excelling in feature extraction and demonstrating the power in handling complex edge structures.

Despite the impressive advances in feature extraction, traditional deep-learning ED methods often overlook the critical aspect of effective feature selection. To address this gap, the extractor-selector (E-S) framework was recently introduced [Shu, 2025] as a novel solution to enhance edge detection performance. This paradigm integrates a feature selector with a feature extractor to generate more accurate edge maps by pixel-wise feature selection, which has achieved state-of-the-art (SOTA) results in both quantitative evaluations and perceptual quality.

However, the current E-S framework still faces limitations, primarily due to the compression of feature maps during the feature extraction process. As selectors operate on highly compressed feature maps, significant information is lost, which may reduce the overall quality of edge detection. Additionally, while union training has been shown to improve perceptual edge predictions in such a framework, it could lead to suboptimal quantitative results, creating a trade-off between perceptual accuracy and quantitative performance. These challenges highlight the need for improving feature selection and training strategies in the E-S method.

To address these limitations, we explore two key aspects in this paper: (1) an enhancement of the E-S architecture to better leverage the feature extraction capabilities of pre-existed extractors, and (2) the introduction of a novel loss function that facilitates perceptual edge predictions, while maintaining SOTA quantitative results, for the E-S method. In detail, on one hand, we propose an enhanced E-S architecture that improves the effectiveness of feature selection by utilizing richer, less-compressed intermediate features as well as extra

features. Specifically, we modify the feature extractor to output more detailed intermediate features prior to fusion, providing the selector with a broader set of options for more precise feature selection. Additionally, we introduce additional feature maps that highlight high-confidence edge and non-edge regions, improving the ability of the selector to refine predictions. These architectural modifications significantly enhance the accuracy of edge detection, as validated through extensive experimental evaluations. On the other hand, we introduce the Symmetrization Weight Binary Cross-Entropy (SWBCE) loss function, which emphasizes both the recall of edge pixels and the suppression of incorrect predictions for non-edge pixels, thereby enhancing perceptual accuracy while preserving competitive quantitative performance. Unlike previous perceptual loss functions, which require manual tuning of hyperparameters across different datasets and models and often at the cost of quantitative performance, SWBCE offers a uniform set of hyperparameters, ensuring broader applicability across diverse datasets while minimizing the trade-off between perceptual quality and quantitative accuracy. The effectiveness and superiority of SWBCE loss function are also demonstrated by extensive experiments.

The key contributions of this work are as follows:

**(1) Enhanced E-S Architecture:** We introduce modifications to the feature extractor to reduce information loss. The proposed architecture outputs richer intermediate features and incorporates additional feature maps, improving edge detection accuracy.

**(2) Novel Loss Function (SWBCE):** We design the Symmetrization Weight Binary Cross-Entropy (SWBCE) loss function, which simultaneously emphasizes edge recall and error suppression for non-edge pixels. SWBCE significantly enhances perceptual edge quality while maintaining SOTA evaluation scores in the E-S framework, without the need for dataset-specific or model-specific tuning of hyperparameters, allowing a broader applicability.

**(3) Extensive Experimental Validation:** We conduct comprehensive experiments on benchmark datasets (BIPED2, BRIND, and UDED) to demonstrate the superiority of our proposed methods over baseline models, the standard E-S framework, and conventional WBCE loss functions. Our approaches demonstrate improvements in both quantitative accuracy and perceptual quality, setting a new benchmark in edge detection.

The remainder of the paper is structured as follows: Section 2 reviews related work on edge detection, including datasets, CNN-based models, the E-S framework, and prior efforts on loss functions. Section 3 details the proposed methodology, including the enhanced E-S architecture and the SWBCE loss function. Section 4 presents experimental results and analysis, followed by conclusions and further works in Section 5.

## 2 Previous Works

This section provides an overview of related work in the domains of datasets, ED models, the E-S paradigm, and loss functions, providing a review of their contributions and limitations.

### 2.1 Datasets

In the early stages of ED research, the task was often conflated with related problems such as contour detection, boundary detection, and segmentation. Consequently, early edge detection studies leveraged datasets that were not explicitly designed for ED but were adapted from other tasks. Notable among these is the Berkeley Segmentation Dataset (BSDS300) and its extended version BSDS500 [Martin *et al.*, 2001], which include 300 and 500 RGB images, respectively, with contour annotations from multiple human annotators. Similarly, the Multi-cue Boundary Dataset (MDBD) [Mély *et al.*, 2016] provides 100 high-resolution images annotated with boundary information across a variety of scenes, while the NYU Depth Dataset (NYUD) and its extension NYUD2 [N. Silberman *et al.*, 2012] contain 1,449 images with segmentation labels. Other widely utilized datasets include PASCAL VOC [Everingham *et al.*, 2010], Microsoft COCO [Lin *et al.*, 2014], SceneParse150 [Zhou *et al.*, 2017], and Cityscapes [Cordts *et al.*, 2016]. While these datasets have been instrumental in the advancement of ED, their primary focus on other vision tasks limits their specificity and applicability to modern ED researches.

As ED matured as an independent research area, more specialized datasets were created to address the unique requirements of the task. The BIPED dataset, later refined into BIPED2 [Soria *et al.*, 2020], includes 250 high-resolution images with single-edge annotations. The BRIND dataset [Pu *et al.*, 2021] re-annotates the BSDS500 dataset, categorizing edges into four distinct types, thus enhancing its utility for more nuanced ED tasks. The UDED dataset [Soria *et al.*, 2023a], consisting of 29 carefully selected images with high-quality edge annotations, further contributes to the benchmark suite for ED.

A persistent challenge in all ED datasets is the reliance on human annotations for groundtruth labeling. Such labels are inherently noisy, often containing missing edges, errors, or inconsistencies. Furthermore, annotation uncertainty arises when different annotators produce divergent results for the same image, or even when the same annotator annotates the same image twice. To mitigate these issues, recent studies have focused on improving annotation quality through advanced labeling techniques and developing models robust to noisy annotations [Fu and Guo, 2023][Wang *et al.*, 2024][Shu, 2024].

### 2.2 Models

The evolution of ED methodologies can be broadly categorized into three phases: heuristic-based methods, statistical approaches, and deep learning-based methods.

#### Heuristic-Based Methods:

Early ED techniques relied on simple heuristic criteria such as intensity gradients to design efficient computational algorithms. Prominent methods include the Sobel operator [Kittler, 1983] and the Canny detector [Canny, 1986], which have remained influential due to their simplicity and effectiveness. Despite their historical significance, these methods face limitations in adaptability to diverse datasets, as their fixed coefficients are often insufficient to distinguish edges from textures in complex datasets.

### Statistical and Early Learning-Based Methods:

In the second phase, statistical and learning-based methods were introduced to improve ED by incorporating hand-crafted features such as Chernoff information [Konishi *et al.*, 2003], histograms [Arbeláez *et al.*, 2011], textures [Martin *et al.*, 2004], and sketch tokens [Lim *et al.*, 2013]. Techniques such as structured forests [Dollár and Zitnick, 2015], nearest-neighbor search [Ganin and Lempitsky, 2014], and logistic regression [Ren, 2008] were employed to classify pixels or patches as edge or non-edge. These approaches demonstrated improved robustness and accuracy compared to heuristic methods, yet their reliance on manual feature engineering constrained scalability and limited their generalization to a wider range of datasets.

### Deep Learning-Based Methods:

The third and current phase has been driven by the emergence of deep learning, particularly convolutional neural networks (CNNs). CNN-based models have revolutionized edge detection by facilitating hierarchical feature extraction and enabling end-to-end learning. One of the pioneering models in this phase, Holistically-Nested Edge Detection (HED) [Xie and Tu, 2015], introduced multi-scale feature learning, where features from various network layers are fused to improve edge prediction. The Richer Convolutional Features (RCF) model [Liu *et al.*, 2017] extended this concept by incorporating features from multiple levels within the same layer to achieve finer ED. Subsequent models such as Bi-Directional Cascade Networks (BDCN) [He *et al.*, 2022], Pixel Difference Networks (PiDiNet) [Su *et al.*, 2021], and Dense Extreme Inception Networks (Dexi) [Soria *et al.*, 2023b] have further advanced edge detection through innovations in architecture, supervision, and feature fusion strategies.

### 2.3 The Extractor-Selector Paradigm

Most existing edge detection models primarily focus on feature extraction while giving less attention to feature selection. Traditional deep learning models rely on computationally expensive feature extractors, followed by simple aggregation techniques, such as  $1 \times 1$  convolution layers, to fuse features. While effective, this approach often falls short in complex ED tasks, as it does not adequately select the most relevant features from the extracted ones.

To address this gap, the E-S paradigm was recently proposed [Shu, 2025]. This framework retains traditional feature extractors but introduces a dedicated selector that processes multi-scale features to produce final edge maps. The selector improves overall performance, both accuracy and perceptual quality, by selecting the most pertinent features for edge predictions.

However, in the original implementation of the E-S paradigm, only the final-layer outputs of the feature extractor were selected, a design choice that provided simplicity but also limited the framework’s potential for further performance gains. Drawing inspiration from models like RCF [Liu *et al.*, 2017], which utilize richer features from multiple layers, a more effective strategy would involve providing the selector with richer, less-compressed features to further improve the performance.

### 2.4 Loss Functions

The (imbalance version of) Weighted Binary Cross-Entropy (WBCE) loss function is the most widely used one in ED. However, WBCE often requires post-processing techniques such as Non-Maximum Suppression (NMS) to refine the edge predictions and enhance perceptual quality. To address these limitations, alternative loss functions have been explored, including Dice loss [Deng *et al.*, 2018], which balances edge preservation with the suppression of the total edge-pixels in the predictions, and tracing loss [Huan *et al.*, 2022], which separates the loss calculation between edge pixels and background textures to strengthen the predicted edges.

Another challenge arises from the imbalance between positive and negative samples in ED data, which can undermine model performance. To mitigate this, besides the imbalance design of WBCE, loss functions like AP-loss [Chen *et al.*, 2019][Cetinkaya *et al.*, 2024] have been introduced to improve prediction accuracy.

Despite these advancements, the adoption of perceptual-improving loss functions often involves trade-offs, such as reduced precision or the need for cumbersome hyperparameter tuning across different datasets and models. These issues restrict the general applicability of these loss functions. Thus, the design of loss functions that can simultaneously optimize both quantitative evaluation and perceptual quality, without requiring dataset-specific and model-specific hyperparameter adjustments, remains a challenging yet important area of research.

## 3 Methodology

This section provides the main schemes of the work, including the enhanced E-S architecture and the SWBCE loss function. For more technical details, please refer to the codes.

### 3.1 The Enhanced E-S Architecture

The proposed architecture builds upon the E-S paradigm described in [Shu, 2025]. As illustrated in Figure 1, the paradigm consists of two key components: the feature extractor and the feature selector. The extractor generates feature maps, which are then selected by the selector to produce the final edge predictions.

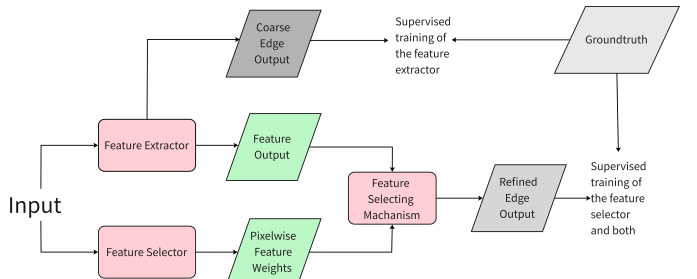
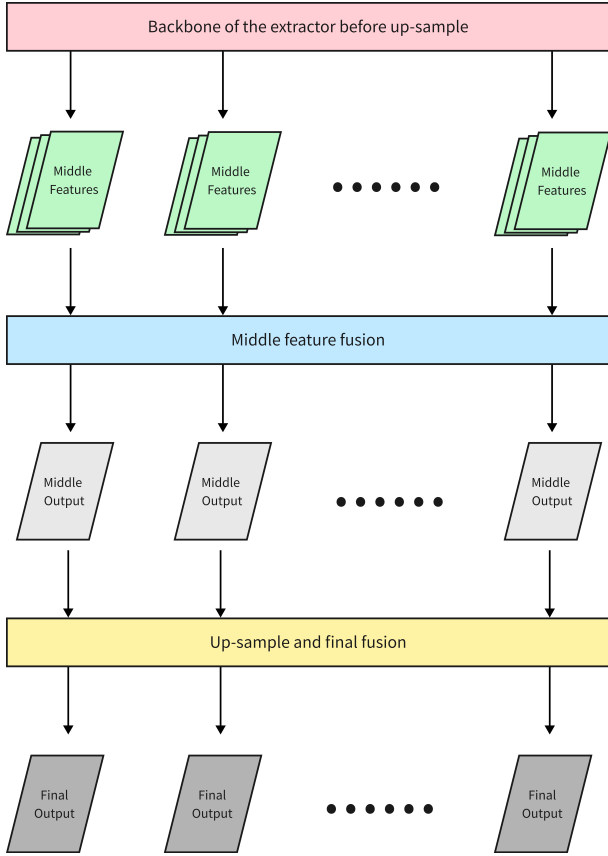


Figure 1: **The framework of the E-S paradigm.** It consists of two components: a feature extractor which produces coarse edge maps and features, and a feature selector which selects multi-scale features for refinements, ultimately outputting the final edge predictions.

To enhance the performance of the E-S architecture, we introduce several modifications, both in the extractor and the

selector. Specifically, we modify the selector only in the final convolutional layer to adjust the number of output channels, while the extractor undergoes more substantial changes, particularly in the up-sampling and fusion layers. These modifications aim to provide richer features with reduced information loss, providing more options for the selector.

In previous models, extractors typically consist of a backbone network with down-sampling blocks that progressively reduce spatial resolution. Multi-scale features are then obtained, fused to one or two edge maps in each scale, and passed through up-sampling blocks to generate final features, at the target resolution, which are further fused to produce the final edge map. Although this structure has been effective in many cases, the final features often suffer from significant information loss and lack of diversity due to the compressed fusion schemes before up-sampling. To address this issue, we modify the up-sampling and fusion layers of the extractor, while preserving the backbone architecture.



**Figure 2: The standard extractor architecture.** The backbone network performs down-sampling to extract multi-scale features. These features are then fused into one or two edge maps at each scale, followed by up-sampling to match the original image resolution. The final prediction is obtained by fusing these resized maps.

Figures 2 and 3 illustrate the differences between the original and modified extractor architectures. In the original architecture (Figure 2), features are fused at multiple scales and up-sampled to the target resolution for prediction. In con-

trast, the modified architecture (Figure 3) integrates multi-scale features into a suitable number of channels, which are then up-sampled without fusion. The up-sampled features are used as the output, offering richer information with reduced loss for selection. Although the final outputted features are still fused into coarse edge maps for pre-training the extractor, it is the unfused features that are used by the selector for the final predictions. Additionally, we introduce two fixed feature maps (one of zeros and one of ones) to assist the selector in making more confident decisions, particularly in cases where a pixel is strongly classified as belonging to either the edge or non-edge region.

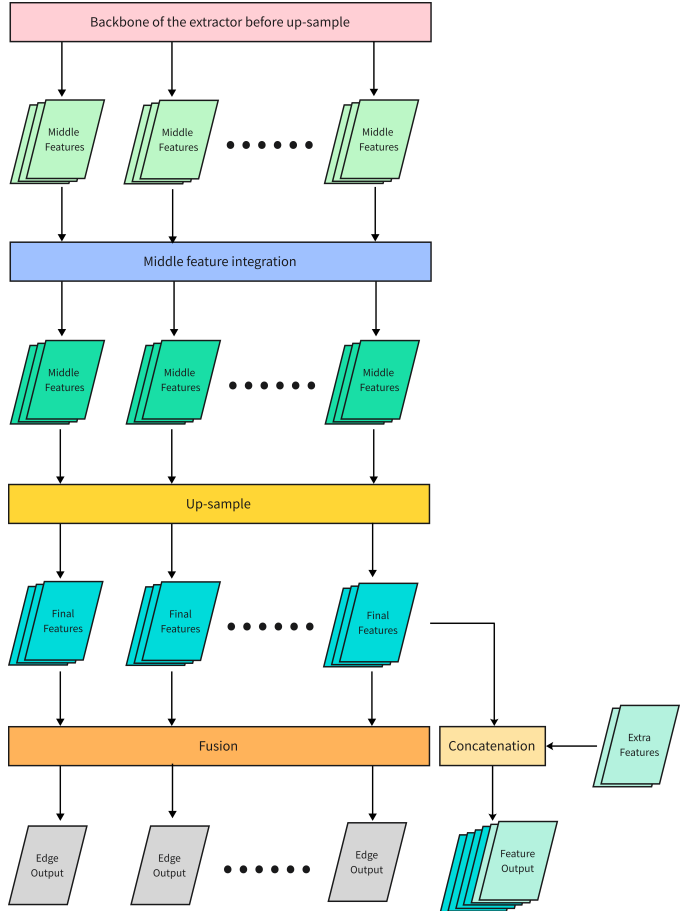


**Figure 3: The modified feature extractor architecture.** This architecture extracts multi-scale features using the same backbone as the standard extractor. However, the extracted features are processed before fusion. They are integrated into a suitable number of channels, and are up-sampled without fusion. Additionally, two fixed feature maps (one of the zeros and one of the ones) are added to the up-sampled features to form the final outputted features, assisting in selecting highly confident pixels, both for edge and non-edge. Although the up-sampled features are also fused to generate coarse edge maps, only being employed in pre-training the extractor, it is the final unfused features rather than the fused ones that are employed by the selector to produce the final predictions.

### 3.2 The SWBCE Loss Function

While WBCE achieves high performance in terms of recall and precision, it struggles to suppress the most challenging pixels, which contribute significantly to blurred edges or polluted non-edge regions. Specifically, non-edge pixels near edges often exhibit similar behavior to edge pixels due to their proximity, resulting in blurred edges, while textural regions may contain prominent features that mimic edges, leading to polluted predictions. These pixels (called the challenging pixels) are impactful but particularly difficult to suppress. During training, WBCE tends to reduce the loss for other pixels instead of focusing on these more impactful but challenging ones, arising from the differential difficulty of suppression.

To mitigate these limitations, the Symmetrization Weighted Binary Cross-Entropy (SWBCE) loss function is designed by emphasizing both the suppression of the challenging pixels and the recall of edge pixels. Observing that the challenging pixels are non-edge ones which however are predicted to be edges, the key insight behind SWBCE then lies in assigning higher weights to predicted edge pixels. This aligns with the discriminative nature of ED that generally, a pixel is viewed as an edge one **only if** there is strong evidence supporting its classification, whereas a pixel is classified as a non-edge one **by default unless evidence suggests otherwise**.

Finally, to leverage existing methods effectively, the SWBCE loss is formulated as the weighted average of two terms: the standard WBCE loss, weighted by ground-truth labels to recall edges, and a loss function symmetrical to the standard WBCE, weighted by predictions to suppress non-edges. Formally, SWBCE is defined as:

$$L_{SWBCE}(\hat{Y}, Y) = \frac{L_{Label}(\hat{Y}, Y) + b \times L_{Pred}(\hat{Y}, Y)}{1 + b} \quad (1)$$

where,  $L_{Label}$  is the standard WBCE loss function, while  $L_{Pred}$  is novelly designed by symmetrizing the WBCE loss function, weight by predictions, and  $b$  is a hyperparameter balancing  $L_{Label}$  and  $L_{Pred}$ , typically set to 1:

$$\begin{aligned} L_{Label}(\hat{Y}, Y) &= - \sum_{y_i \in Y} \alpha_i [y_i \log(\hat{y}_i) + (1 - y_i) \log(1 - \hat{y}_i)] \\ &= -\alpha \sum_{y_i \in Y^+} \log(\hat{y}_i) - \lambda(1 - \alpha) \sum_{y_i \in Y^-} \log(1 - \hat{y}_i) \end{aligned} \quad (2)$$

where,  $\hat{y}_i$  is the pixel in the prediction  $\hat{Y}$  corresponding to the pixel  $y_i$  in the groundtruth  $Y$ ,  $Y^+$  is the set of edge pixels in  $Y$  (positive samples),  $Y^-$  is the set of non-edge pixels in  $Y$  (negative samples). For  $y_i \in Y^+$ ,  $\alpha_i = \alpha = \frac{|Y^-|}{|Y|}$  and for  $y_i \in Y^-$ ,  $\alpha_i = \lambda(1 - \alpha)$  are their weights, respectively.  $\lambda = 1.1$  as suggested in previous works. And:

$$L_{Pred}(\hat{Y}, Y) = - \sum_{\hat{y}_i \in \hat{Y}} \hat{\alpha}_i [y_i \log(\hat{y}_i) + (1 - y_i) \log(1 - \hat{y}_i)] \quad (3)$$

where,

- $\hat{\alpha}_i = \hat{y}_i \frac{\hat{I}_N}{|\hat{Y}|} + (1 - \hat{y}_i) \hat{\lambda} \frac{\hat{I}_P}{|\hat{Y}|}$  is the weight of the pixel  $\hat{y}_i$ .

- $\hat{I}_P = \sum_{\hat{y}_i \in \hat{Y}} \hat{y}_i$  is the influence of predicted edges

- $\hat{I}_N = |\hat{Y}| - \hat{I}_P$  is the influence of predicted non-edges.

- $\hat{\lambda} = 1.1$  is a balancing hyperparameter as  $\lambda$  in  $L_{Label}$ .

The SWBCE loss function emphasizes both the recall of edge pixels by  $L_{Label}$  and the error suppression of the challenging pixels by  $L_{Pred}$ . The latter is a symmetry of the former, weighting by predictions to focus on suppressing errors on non-edge pixels, while it has also considered the imbalance of edges and non-edges in the prediction, as the standard WBCE did for groundtruths.

### 3.3 Training Methods

To assess of the enhanced E-S architecture and SWBCE loss function, various training schemes are utilized.

To compare the performance of the enhanced E-S architecture with baseline models and the standard E-S architecture, a three-stage training process is adopted, following [Shu, 2025], including (1) Pre-train the feature extractor using its default loss function, (2) Train the feature selector using WBCE loss function with frozen coefficients of the extractor, and (3) Union train the extractor and selector, also using the WBCE loss function.

And to evaluate the proposed SWBCE loss function, the enhanced E-S architecture is also trained with the SWBCE loss function without stage (3), since the simplified process has enabled the models to achieve both high quantitative performance and satisfactory perceptual quality.

## 4 Experiments

This section presents the evaluations of the proposed methods on dataset BIPED2, UDED, and BRIND, where three previous models, HED, BDCN, and Dexi, are employed as baseline models and extractors.

### 4.1 Benchmarks

The quantitative evaluation follows the algorithm presented in [Martin *et al.*, 2004], measuring the Optimal Dataset Scale (ODS), Optimal Image Scale (OIS), and Average Precision (AP), under set error toleration distances. However, the error toleration distance is set to be the stringest 1-pixel as suggested in [Shu, 2024], in contrast to the traditional 4 to 11 pixels, for a high standard. Moreover, all evaluations were conducted without post-processing such as NMS, and data is processed similarly as in [Shu, 2025].

The proposed E-S models were evaluated against baseline models without selectors, as well as those based on the standard E-S architecture, using the WBCE loss function. Additionally, the SWBCE loss function was assessed in comparison to WBCE loss function in the enhanced E-S architectures.

### 4.2 Experiment Results

The quantitative results are summarized in Tables 1 with representative visual predictions shown in Figure 4. They consistently demonstrate the effectiveness of the proposed methods. Across all datasets, the proposed methods yield the most significant performance improvements, underscoring their superior performance. In details:

	BIPED2			UDED			BRIND		
	ODS	OIS	AP	ODS	OIS	AP	ODS	OIS	AP
HED	0.592	0.602	0.347	0.716	0.751	0.489	0.645	0.656	0.417
HED-S	0.649	0.654	0.433	0.733	0.764	0.521	0.668	0.677	0.466
	(+9.63%)	(+8.64%)	(+24.78%)	(+2.37%)	(+1.73%)	(+6.54%)	(+3.57%)	(+3.20%)	(+11.75%)
HED-RS	<b>0.666</b>	<b>0.671</b>	<b>0.493</b>	<b>0.738</b>	<b>0.765</b>	<b>0.635</b>	<b>0.679</b>	<b>0.687</b>	<b>0.492</b>
	(+12.50%)	(+11.46%)	(+42.07%)	(+3.07%)	(+1.86%)	(+29.86%)	(+5.27%)	(+4.73%)	(+17.98%)
HED-S -U	0.655	0.663	<b>0.491</b>	0.723	0.751	0.602	0.668	0.673	0.522
	(+10.64%)	(+10.13%)	(+41.50%)	(+0.98%)	(+0.00%)	(+23.11%)	(+3.57%)	(+2.59%)	(+25.18%)
HED-RS -U	<b>0.659</b>	<b>0.665</b>	0.490	<b>0.754</b>	<b>0.782</b>	<b>0.616</b>	<b>0.669</b>	<b>0.676</b>	<b>0.543</b>
	(+11.32%)	(+10.45%)	(+41.21%)	(+5.31%)	(+4.13%)	(+25.97%)	(+3.72%)	(+3.05%)	(+30.22%)
HED-RS -SWBCE	<b>0.667</b>	<b>0.674</b>	<b>0.543</b>	<b>0.774</b>	<b>0.787</b>	<b>0.661</b>	<b>0.681</b>	<b>0.691</b>	<b>0.594</b>
	(+12.67%)	(+11.96%)	(+56.48%)	(+9.42%)	(+4.79%)	(+35.17%)	(+5.58%)	(+5.34%)	(+42.45%)
BDCN	0.629	0.635	0.421	0.706	0.744	0.530	0.659	0.672	0.467
BDCN-S	0.633	0.639	0.423	0.727	0.764	0.569	0.668	0.677	0.486
	(+0.64%)	(+0.63%)	(+0.46%)	(+2.97%)	(+2.69%)	(+7.36%)	(+1.37%)	(+0.74%)	(+4.07%)
BDCN-RS	<b>0.652</b>	<b>0.655</b>	<b>0.473</b>	<b>0.750</b>	<b>0.777</b>	<b>0.628</b>	<b>0.678</b>	<b>0.686</b>	<b>0.521</b>
	(+3.66%)	(+3.15%)	(+12.35%)	(+6.23%)	(+4.44%)	(+18.49%)	(+2.88%)	(+2.08%)	(+10.92%)
BDCN-S -U	<b>0.661</b>	<b>0.666</b>	<b>0.484</b>	0.758	<b>0.778</b>	<b>0.625</b>	0.672	<b>0.681</b>	0.516
	(+5.09%)	(+4.88%)	(+14.96%)	(+7.37%)	(+4.57%)	(+17.92%)	(+1.97%)	(+1.34%)	(+10.49%)
BDCN-RS -U	0.652	0.660	0.462	<b>0.762</b>	<b>0.778</b>	0.623	<b>0.676</b>	<b>0.681</b>	<b>0.536</b>
	(+3.66%)	(+3.94%)	(+9.74%)	(+7.93%)	(+4.57%)	(+17.55%)	(+2.58%)	(+1.34%)	(+14.78%)
BDCN-RS -SWBCE	<b>0.662</b>	<b>0.666</b>	<b>0.515</b>	0.749	0.777	<b>0.670</b>	0.673	0.684	<b>0.566</b>
	(+5.25%)	(+4.88%)	(+22.33%)	(+6.09%)	(+4.44%)	(+26.42%)	(+2.12%)	(+1.79%)	(+21.20%)
Dexi	0.632	0.636	0.432	0.733	0.752	0.600	0.666	0.672	0.478
Dexi-S	0.640	0.644	0.441	0.737	0.759	0.598	0.671	0.678	0.485
	(+1.27%)	(+1.26%)	(+2.08%)	(+0.55%)	(+0.93%)	(-0.33%)	(+0.75%)	(+0.89%)	(+1.46%)
Dexi-RS	<b>0.672</b>	<b>0.677</b>	<b>0.499</b>	<b>0.784</b>	<b>0.796</b>	<b>0.683</b>	<b>0.683</b>	<b>0.691</b>	<b>0.490</b>
	(+6.33%)	(+6.45%)	(+15.51%)	(+6.96%)	(+5.85%)	(+13.83%)	(+2.55%)	(+2.83%)	(+2.51%)
Dexi-S -U	0.650	0.656	<b>0.465</b>	0.771	0.786	<b>0.629</b>	<b>0.666</b>	<b>0.673</b>	<b>0.529</b>
	(+2.89%)	(+3.14%)	(+7.64%)	(+5.18%)	(+4.52%)	(+4.83%)	(+0.00%)	(+0.15%)	(+10.04%)
Dexi-RS -U	<b>0.651</b>	<b>0.657</b>	0.463	<b>0.780</b>	<b>0.797</b>	0.601	0.662	0.669	0.521
	(+3.01%)	(+2.99%)	(+7.18%)	(+6.41%)	(+5.98%)	(+0.17%)	(-0.60%)	(-0.45%)	(+9.00%)
Dexi-RS -WBCE	<b>0.677</b>	<b>0.681</b>	<b>0.540</b>	0.774	<b>0.799</b>	<b>0.714</b>	0.682	0.689	<b>0.566</b>
	(+7.12%)	(+7.08%)	(+25.00%)	(+5.59%)	(+6.25%)	(+19.00%)	(+2.40%)	(+2.53%)	(+18.41%)
A	0.618	0.624	0.400	0.718	0.749	0.540	0.657	0.667	0.454
A-S	0.641	0.646	0.432	0.732	0.761	0.562	0.669	0.675	0.479
	(+3.72%)	(+3.53%)	(+8.00%)	(+1.95%)	(+1.60%)	(+4.07%)	(+1.83%)	(+1.20%)	(+5.51%)
A-RS	<b>0.663</b>	<b>0.668</b>	<b>0.488</b>	<b>0.757</b>	<b>0.779</b>	<b>0.649</b>	<b>0.680</b>	<b>0.688</b>	<b>0.501</b>
	(+7.28%)	(+7.05%)	(+22.00%)	(+5.43%)	(+4.01%)	(+20.19%)	(+3.50%)	(+3.15%)	(+10.35%)
A-S -U	<b>0.655</b>	<b>0.662</b>	<b>0.480</b>	0.751	0.772	<b>0.619</b>	<b>0.669</b>	<b>0.676</b>	<b>0.533</b>
	(+6.02%)	(+6.09%)	(+20.00%)	(+4.60%)	(+3.07%)	(+14.63%)	(+1.83%)	(+1.35%)	(+17.40%)
A-RS -U	0.654	0.661	0.472	<b>0.765</b>	<b>0.786</b>	0.613	<b>0.669</b>	0.675	<b>0.533</b>
	(+5.83%)	(+5.93%)	(+18.00%)	(+6.55%)	(+4.94%)	(+13.52%)	(+1.83%)	(+1.20%)	(+17.40%)
A-RS -SWCE	<b>0.669</b>	<b>0.674</b>	<b>0.533</b>	<b>0.766</b>	<b>0.788</b>	<b>0.682</b>	0.679	<b>0.688</b>	<b>0.575</b>
	(+8.25%)	(+8.01%)	(+33.25%)	(+6.69%)	(+5.21%)	(+26.30%)	(+3.35%)	(+3.15%)	(+26.65%)

Table 1: **Results on BIPED2, UDED, and BRIND with 1-pixel error tolerance without NMS:** The 1-pixel error tolerance corresponds to the strictest evaluation setting, with the error toleration distance in the evaluation algorithm set to 0.003 for the BRIND and UDED datasets, and 0.001 for BIPED2, respectively. This is a marked reduction from the default tolerance of 0.0075, which translates to 4.3 pixels for BRIND and 11.1 pixels for BIPED2. Notations such as *-S* and *-S-U* indicate the results of the standard E-S architecture without and with union training, respectively, while *-RS* and *-RS-U* correspond to the enhanced E-S architecture proposed in this work, with and without union training, respectively, using WBCE loss function. In addition, *-RS-SWBCE* represents the result of enhanced E-S architecture with the employment of SWBCE loss function, and *A* represents that the results of averaging over the three baseline models. The improvements relative to the use of each baseline model (extractor) alone are denoted in parentheses. The better score between the enhanced E-S architecture and the standard E-S architecture without or with union training is **bolded**, respectively, while best scores among all are **bolded and italicized**, respectively in each extractor as well as the average.

## Quantitative Analysis

For the BIPED2 with the WBCE loss function and without the union training, the proposed architecture achieves average improvements of 7.28%, 7.05%, and 22.00% in ODS, OIS, and AP, respectively, when compared to models without selectors. In contrast, models employing the standard E-S architecture show relatively modest improvements of 3.72%, 3.53%, and 8.00%, respectively. Moreover, by employing the SWBCE loss function, the proposed architecture achieves further improvements of 8.25%, 8.01%, and 33.25%, respectively, outperforming the former ones.

For the UDED dataset with the WBCE loss function and without the union training, the proposed architecture achieved notable gains of 5.43%, 4.01%, and 20.19% in ODS, OIS, and AP, respectively. In contrast, the standard E-S architecture produced smaller improvements of 1.95%, 1.60%, and 4.07%. Moreover, by employing the SWBCE loss function, the proposed E-S architecture achieves further improvements of 6.69%, 5.21%, and 26.30%, respectively, also outperforming the former ones.

For the BRIND dataset with the WBCE loss function and without the union training, the proposed architecture exhibits improvements of 3.50%, 3.15%, and 10.35% for ODS, OIS, and AP, respectively, compared to models without selectors. By comparison, models employing the standard E-S architecture yield gains of 1.83%, 1.20%, and 5.51%, respectively. Moreover, by employing the SWBCE loss function, the proposed E-S architecture achieves improvements of 3.35%, 3.15%, and 26.65%, respectively, competitive on ODS and OIS while better on AP compared to the former ones.

## Qualitative Analysis

Figure 4 presents visual comparisons of the predicted outputs. It showcases full images alongside cropped regions (the blue and yellow boxes). The rows represent the original images, groundtruths, and model predictions, respectively. Notably, the proposed enhanced E-S architecture generates more perceptual edge predictions compared to both the standard E-S architecture and the baseline model, using WBCE loss function, while the usage of SWBCE loss function further and significantly improves the performance.

## 5 Conclusion and Further Works

In this paper, we have presented an enhanced framework of the E-S paradigm originally presented in [Shu, 2025] for ED, designed to overcome the limitations of the standard one that insufficiently utilizes feature representations during the selection process. Additionally, we have presented the SWBCE loss function, aiming to simultaneously achieve SOTA quantitative scores and perceptual quality, for the same tasks. By leveraging richer and less-loss feature representations and incorporating extra features, the proposed enhanced E-S architecture provides a more effective solution for ED tasks, achieving significant improvements, while by emphasizing both recall of the edges and suppressing erroneously predicted edges, the SWBCE loss function offers an advanced method for generating high-quality edge predictions both quantitative and perceptual. The effectiveness and superiority of both schemes are confirmed by extensive experiments

over various datasets and baseline models. Notably, the enhanced E-S architecture combined with SWBCE achieved an average improvement of about 8.25%, 8.01%, and 33.25% on ODS, OIS, and AP, respectively on BIPED2 dataset compared to the baseline models. These findings establish new benchmarks for ED tasks, and indicate the potential of the methods for border application in beyond.

Despite these notable achievements, several avenues for further research remain. First, designing specific extractors based on the E-S architecture rather than directly accessing previous ones might provide a more effective solution for ED. Second, the computational efficiency of the standard and enhanced E-S architectures could be improved to better support resource-constrained scenarios such as real-time edge detection for high-resolution images, which would make the framework more practical for applications like autonomous systems. Additionally, the SWBCE loss function could be further optimized to achieve even more precise edge predictions or adapted for related tasks such as semantic segmentation. Nevertheless, the presented work provides exciting opportunities for advancing ED and further tasks.

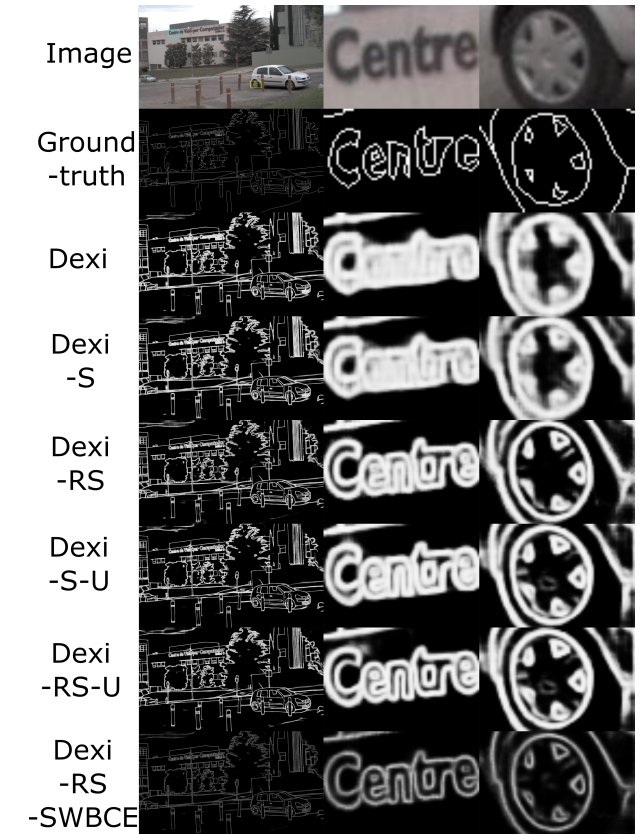


Figure 4: **Visual comparisons.** Columns 1 presents the full images, while columns 2 and 3 display the corresponding cropped regions marked by blue (the up-left words) and yellow boxes (the down-right tire), respectively. The rows represent the original images, groundtruths, and model predictions. The notations follow Table 1. Obviously, the enhanced E-S framework trained by the SWBCE loss function obtains the most perceptual predictions.

## 6 References

### References

[Arbeláez *et al.*, 2011] P. Arbeláez, M. Maire, C. Fowlkes, and J. Malik. Contour detection and hierarchical image segmentation. *IEEE Transactions on Pattern Analysis and Machine Intelligence*, 33(5):898–916, 2011.

[Canny, 1986] J. Canny. A computational approach to edge detection. *IEEE Transactions on pattern analysis and machine intelligence*, PAMI-8(6):679–698, 1986.

[Cetinkaya *et al.*, 2024] B. Cetinkaya, S. Kalkan, and E. Akbas. Ranked: Addressing imbalance and uncertainty in edge detection using ranking-based losses. In *Proceedings of the IEEE/CVF Conference on Computer Vision and Pattern Recognition*, pages 3239–3249, 2024.

[Chen *et al.*, 2019] K. Chen, J. G. Li, W. Y. Lin, J. See, J. Wang, L. Y. Duan, Z. B. Chen, C. W. He, and J. N. Zou. Towards accurate one-stage object detection with ap-loss. In *Proceedings of the IEEE/CVF Conference on Computer Vision and Pattern Recognition*, pages 5119–5127, 2019.

[Cordts *et al.*, 2016] M. Cordts, M. Omran, S. Ramos, T. Rehfeld, M. Enzweiler, R. Benenson, U. Franke, S. Roth, and B. Schiele. The cityscapes dataset for semantic urban scene understanding. In *Proceedings of the IEEE Conference on Computer Vision and Pattern Recognition (CVPR)*, June 2016.

[Deng *et al.*, 2018] R. X. Deng, C. H. Shen, S. J. Liu, H. B. Wang, and X. R. Liu. Learning to predict crisp boundaries. In *Computer Vision – ECCV 2018: 15th European Conference, Munich, Germany, September 8–14, 2018, Proceedings, Part VI*, page 570–586. Springer-Verlag, 2018.

[Dollár and Zitnick, 2015] P. Dollár and C. L. Zitnick. Fast edge detection using structured forests. *IEEE Transactions on Pattern Analysis and Machine Intelligence*, 37(8):1558–1570, 2015.

[Everingham *et al.*, 2010] M. Everingham, L. Van Gool, C. K. I. Williams, J. Winn, and A. Zisserman. The pascal visual object classes (voc) challenge. *International Journal of Computer Vision*, 88(2):303–338, jun 2010.

[Fu and Guo, 2023] Y. B. Fu and X. J. Guo. Practical edge detection via robust collaborative learning. In *Proceedings of the 31st ACM International Conference on Multimedia, MM ’23*, page 2526–2534. Association for Computing Machinery, 2023.

[Ganin and Lempitsky, 2014] Y. Ganin and V. Lempitsky.  $n^4$ -fields: neural network nearest neighbor fields for image transforms. In *Asian conference on computer vision*, pages 536–551. Springer, 2014.

[He *et al.*, 2022] J. Z. He, S. L. Zhang, M. Yang, Y. H. Shan, and T. J. Huang. Bdcn: Bi-directional cascade network for perceptual edge detection. *IEEE Transactions on Pattern Analysis and Machine Intelligence*, 44(1):100–113, 2022.

[Huan *et al.*, 2022] L. X. Huan, N. Xue, X. W. Zheng, W. He, J. Y. Gong, and G. S. Xia. Unmixing convolutional features for crisp edge detection. *IEEE Trans. Pattern Anal. Mach. Intell.*, 44(10 Part 1):6602–6609, oct 2022.

[Kittler, 1983] J. Kittler. On the accuracy of the sobel edge detector. *Image and Vision Computing*, 1(1):37–42, 1983.

[Konishi *et al.*, 2003] S. Konishi, A. L. Yuille, J. M. Coughlan, and S. C. Zhu. Statistical edge detection: learning and evaluating edge cues. *IEEE Transactions on Pattern Analysis and Machine Intelligence*, 25(1):57–74, 2003.

[Lim *et al.*, 2013] J. J. Lim, C. L. Zitnick, and P. Dollár. Sketch tokens: A learned mid-level representation for contour and object detection. In *Proceedings of the IEEE conference on computer vision and pattern recognition*, pages 3158–3165, 2013.

[Lin *et al.*, 2014] T. Y. Lin, M. Maire, S. Belongie, L. Bourdev, R. Girshick, J. Hays, P. Perona, D. Ramanan, C. L. Zitnick, and P. Dollár. Microsoft coco: Common objects in context. In *Computer Vision – ECCV 2014*, pages 740–755. Springer International Publishing, 2014.

[Liu *et al.*, 2017] Y. Liu, M. M. Cheng, X. W. Hu, K. Wang, and X. Bai. Richer convolutional features for edge detection. In *Proceedings of the IEEE conference on computer vision and pattern recognition*, pages 3000–3009, 2017.

[Martin *et al.*, 2001] D. Martin, C. Fowlkes, D. Tal, and J. Malik. A database of human segmented natural images and its application to evaluating segmentation algorithms and measuring ecological statistics. In *Proc. 8th Int’l Conf. Computer Vision*, volume 2, pages 416–423, July 2001.

[Martin *et al.*, 2004] D.R. Martin, C.C. Fowlkes, and J. Malik. Learning to detect natural image boundaries using local brightness, color, and texture cues. *IEEE Transactions on Pattern Analysis and Machine Intelligence*, 26(5):530–549, 2004.

[Muthukrishnan and Radha, 2011] R. Muthukrishnan and M. Radha. Edge detection techniques for image segmentation. *International Journal of Computer Science & Information Technology*, 3(6):259, 2011.

[Mély *et al.*, 2016] D. A. Mély, J. k. Kim, M. McGill, Y. L. Guo, and T. Serre. A systematic comparison between visual cues for boundary detection. *Vision Research*, 120:93–107, 2016. Vision and the Statistics of the Natural Environment.

[N. Silberman *et al.*, 2012] N. N. Silberman, D. Hoiem, P. P. Kohli, and R. Fergus. Indoor segmentation and support inference from rgbd images. In *European Conference on Computer Vision*, 2012.

[Nazeri *et al.*, 2019] K. Nazeri, E. Ng, T. Joseph, F. Qureshi, and M. Ebrahimi. Edgeconnect: Structure guided image inpainting using edge prediction. In *2019 IEEE/CVF International Conference on Computer Vision Workshop (ICCVW)*, pages 3265–3274, 2019.

[Pu *et al.*, 2021] M. Pu, Y. Huang, Q. Guan, and H. Ling. Rindnet: Edge detection for discontinuity in reflectance, illumination, normal and depth. In *2021 IEEE/CVF International Conference on Computer Vision (ICCV)*, pages 6859–6868. IEEE Computer Society, oct 2021.

[Ren, 2008] X. F. Ren. Multi-scale improves boundary detection in natural images. In *Computer Vision–ECCV*

2008: 10th European Conference on Computer Vision, Marseille, France, October 12-18, 2008, Proceedings, Part III 10, pages 533–545. Springer, 2008.

[Shu, 2024] Hao Shu. More precise edge detections. 2024.

[Shu, 2025] Hao Shu. Pixel-wise feature selection for perceptual edge detection without post-processing. 2025.

[Soria *et al.*, 2020] X. Soria, E. Riba, and A. Sappa. Dense extreme inception network: Towards a robust cnn model for edge detection. In *2020 IEEE Winter Conference on Applications of Computer Vision (WACV)*, pages 1912–1921. IEEE Computer Society, mar 2020.

[Soria *et al.*, 2023a] X. Soria, Y. Li, M. Rouhani, and A. D. Sappa. Tiny and efficient model for the edge detection generalization. In *2023 IEEE/CVF International Conference on Computer Vision Workshops (ICCVW)*, pages 1356–1365. IEEE Computer Society, oct 2023.

[Soria *et al.*, 2023b] X. Soria, A. Sappa, P. Humanante, and A. Akbarinia. Dense extreme inception network for edge detection. *Pattern Recognition*, 139:109461, 2023.

[Su *et al.*, 2021] Z. Su, W. Z. Liu, Z. T. Yu, D. W. Hu, Q. Liao, Q. Tian, M. Pietikäinen, and L. Liu. Pixel difference networks for efficient edge detection. In *Proceedings of the IEEE/CVF international conference on computer vision*, pages 5117–5127, 2021.

[Wang *et al.*, 2024] C. Wang, D. Dai, S. Xia, Y. Liu, and G. Wang. One-stage deep edge detection based on dense-scale feature fusion and pixel-level imbalance learning. *IEEE Transactions on Artificial Intelligence*, 5(01):70–79, jan 2024.

[Xie and Tu, 2015] S. N. Xie and Z. W. Tu. Holistically-nested edge detection. In *Proceedings of the IEEE international conference on computer vision*, pages 1395–1403, 2015.

[Zhan *et al.*, 2007] C. H. Zhan, X. H. Duan, S. Y. Xu, Z. Song, and M. Luo. An improved moving object detection algorithm based on frame difference and edge detection. In *Fourth international conference on image and graphics (ICIG 2007)*, pages 519–523. IEEE, 2007.

[Zhou *et al.*, 2017] B. L. Zhou, H. Zhao, X. Puig, S. Fidler, A. Barriuso, and A. Torralba. Scene parsing through ade20k dataset. In *2017 IEEE Conference on Computer Vision and Pattern Recognition (CVPR)*, pages 5122–5130, 2017.